Natural high-entropy interface with kinetics-boosted and water-desolventized effects for high-performance aqueous zinc ion batteries

Yanxin Li,[a] Hongfeng Jia,[a] Usman Ali,[a] Bingqiu Liu,[a] Lu Li,[*a] Lingyu Zhang,[a] Tingting Wang,[b] and Chungang Wang[*a]

[a] Department of Chemistry, Northeast Normal University, 5268 Renmin Street, Changchun, Jilin 130024, P. R. China

*Corresponding Author Prof. Lu Li; Prof. Chungang Wang

E-mail: lil106@nenu.edu.cn; wangcg925@nenu.edu.cn

Experimental section

Materials: Diatomite, isopropanol (IPA), and Zn foils (purity 99.99%) were purchased from Shanghai Macklin Biochemical Technology Co., Ltd. Polyacrylic acid, zinc sulfate, and manganese sulfate were purchased from Sigma-Aldrich. Zinc oxide (ZnO), potassium permanganate ($KMnO_4$), isopropyl alcohol (IPA), and ethanol were obtained from Sinopharm Chemical Reagent Beijing Co., Ltd. All reagents were used directly without further purification. Deionized water was thoroughly used during the experiment.

Preparation of DTM-Zn: The diatomite and PVDF were homogeneously mixed in NMP in a ratio 9:1. The slurry was uniformly applied to the polished zinc foil and dried in a vacuum oven for 12 h. The electrode was treated at 10 MPa for 2 min.

Preparation of DTM/A-Zn: The diatomite was soaked in 5 M hydrochloric acid for 12 h and then washed repeatedly with water. After drying, it was mixed well with PVDF in NMP in a ratio of 9:1 by mass. The slurry was evenly applied to the polished zinc foil and dried in a vacuum oven for 12 h. The electrodes were subjected to a pressure of 10 MPa for 2 min.

Preparation of SiO_2-Zn: 5 ml tetrabutyl silicate was added to 30 ml DI water. Subsequently, 5 ml concentrated ammonia was added and stirred continuously for 12 h. The resultant SiO_2 nanoparticles were collected by centrifugation and washed thrice with deionized water and isopropanol. After drying, the powder was calcined under Air atmosphere at 800°C for 3 h. Subsequently, the powder was mixed well with PVDF to form a slurry. The slurry was uniformly coated on the polished zinc foil and dried in a

vacuum oven for 12 h. Finally, the electrode was pressed under 10 MPa for 2 min.

Preparation of MnO_2 pre-embedded with potassium ions cathode (KMO): Deionized water (900 ml) was taken in a 3000 mL cone bottle followed by ultrasonic dispersion of 4.5 ml PAA aqueous solution (0.2 g ml^{-1}) and 180 mg ZnO at room temperature. Afterward, the solution was magnetically stirred with dropwise addition of 1800 ml IPA to gain the PAA-Zn NSs suspension. The resultant PAA-Zn NSs suspension was collected by centrifugation and washed three times with deionized water and isopropanol. Subsequently, after drying at 50 ℃ for 12 h, the final powder was labeled as PAA-Zn NSs. Finally, The CNSs were achieved by calcinating the PAA-Zn NSs at 900 °C for 2 h under an Ar atmosphere. 0.2 M $KMnO_4$ solution (70 ml) and 20 mg CNSs were added into a 100 mL Teflon-lined sealed autoclave and reacted at 180 °C for 30 min. After cooling down to room temperature naturally, the harvested product was repeatedly rinsed with deionized water and absolute ethanol, and obtained by drying in a vacuum oven at 80 °C for 12 h.

Preparation of $NH_4V_4O_{10}$: Firstly, 5 mmol NH_4VO_3 was dissolved in 30 ml deionized water. After stirring at room temperature for 30 min, 2 mmol oxalic acid was added with vigorous stirring for 40 min. The mixture was poured into a 50 ml reactor and reacted at 180 ℃ for 6 h. After centrifuging and drying, the dark green $NH_4V_4O_{10}$ powder was obtained.

Battery Assembly: The cathode was coated with a mixture of KMO, acetylene black, and polyvinylidene fluoride (PVDF) binder (mass ratio 7:2:1) mixed well in NMP solvent onto a stainless steel mesh. NMP was dried in a vacuum oven at 80 °C for 12 h

to allow complete volatilization. For Zn/KMO cells, the active material loading of the individual electrode was about 1.8-2.0 mg cm^{-2}. 120 μL aqueous solution of 2 M $ZnSO_4$ and 0.2 M $MnSO_4$ was selected as electrolyte. For Zn/Cu and Zn/Zn symmetric cells, the Cu and Zn electrodes were 12 mm in diameter and the electrolyte was 2 M $ZnSO_4$. For the assembly of cells with electrodes containing HEO-CNFs, the HEO-CNFs, which are a little larger than the zinc foil are placed between the glass fiber membrane and zinc foil.

Electrochemical measurements: The electrochemical impedance spectroscopy (EIS) was collected over the frequency range from 100 kHz to 0.1 Hz by PARSTAT MC 2000 A. Cyclic voltammetry (CV), chromoamperograms (CAs), linear scan voltammetry (LSV), and Tafel plot were tested on the CHI760E electrochemical workstation. CV curves of Zn/KMO cells were performed between 0.80 and 1.80 V at a scan rate of 0.1 mV s^{-1}. LSV curves were conducted by the three-electrodes device at a scan rate of 1 mV s^{-1} in 1 M Na_2SO_4 electrolyte. CAs were collected at an overpotential of -150 mV in coin cells. The galvanostatic cycling performance of Zn/Zn and Zn/Cu was performed in coin cells on a Neware Battery Measurement System (Neware, China). The discharge-charge cycling of Zn/KMO was measured on a battery test instrument (CT2001A, LAND, China) within a voltage range of 0.80-1.80 V.

Materials characterization: X-ray powder diffraction (XRD) analysis was obtained on a D8 Focus diffractometer (Bruker) with Cu-Ka radiation (λ=0.15405 nm). High-resolution transmission electron microscope (HR-TEM) characterizations were taken by JEOLJEM-2100F transmission electron microscope at 200 kV accelerating voltage.

Scanning electron microscopy (SEM) images were measured by an XL30 ESEM-FEG field-emission scanning electron microscope (FEI Co.) with an energy dispersive X-ray spectrum (EDS). Raman spectrum was recorded at room temperature with a JY HR-800 LabRam confocal Raman microscope in a backscattering configuration, with an excitation wavelength of 488 nm. Atom force microscope (AFM) was performed on Asylum Research Cypher ES. Inductively-coupled plasma optical emission spectroscopy (ICP-OES) measurements were conducted to examine the chemical composition. X-ray photoelectron spectrum (XPS) was tested on an ECSALAB 250 using non-monochromatized Al-Kα radiation. A contact angle measuring device was used to test the wettability of materials (DSA 100, KRUSS).

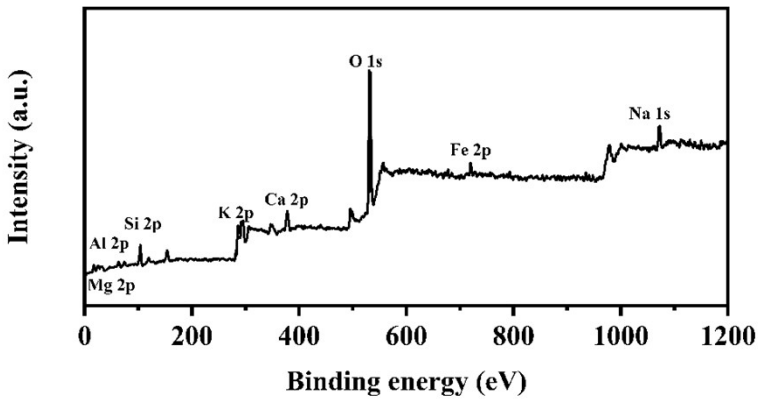

Fig. S1 Survey XPS spectrum of DTM.

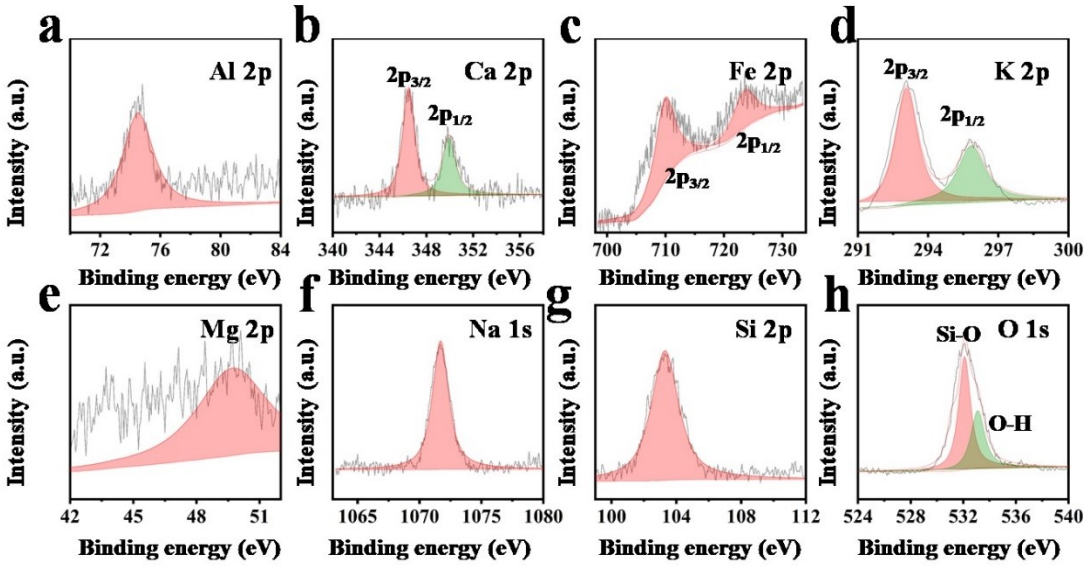

Fig. S2 XPS spectra of DTM for (a) Al 2p, (b) Ca 2p, (c) Fe 2p, (d) K 2p, (e) Mg 2p, (f) Na 1s, (g) Si 2p, and (h) O 1s.

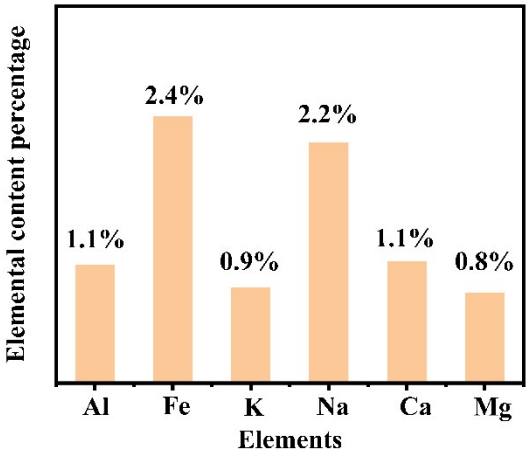

Fig. S3 Contents of metal elements in DTM tested by Inductively coupled plasma (ICP).

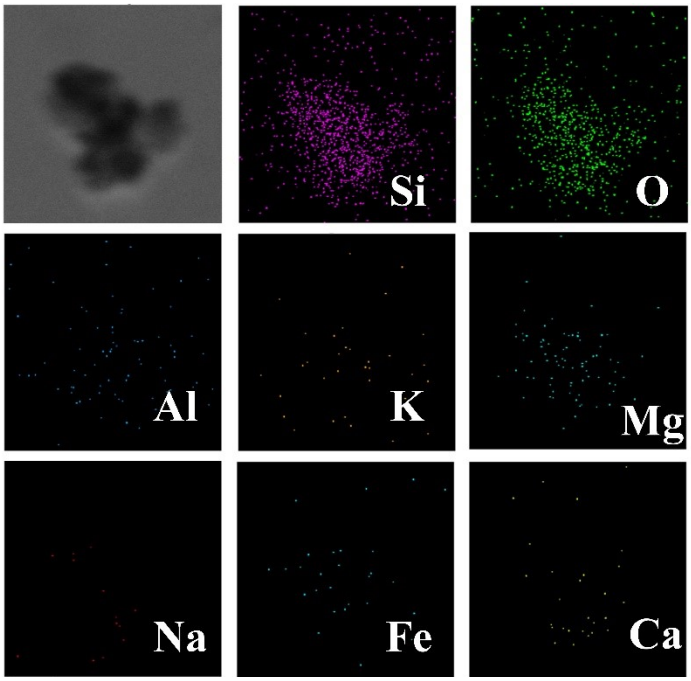

Fig. S4 TEM image and corresponding elemental mapping images of Si, O, K, Ca, Al, Mg, Fe, and Na in DTM/A.

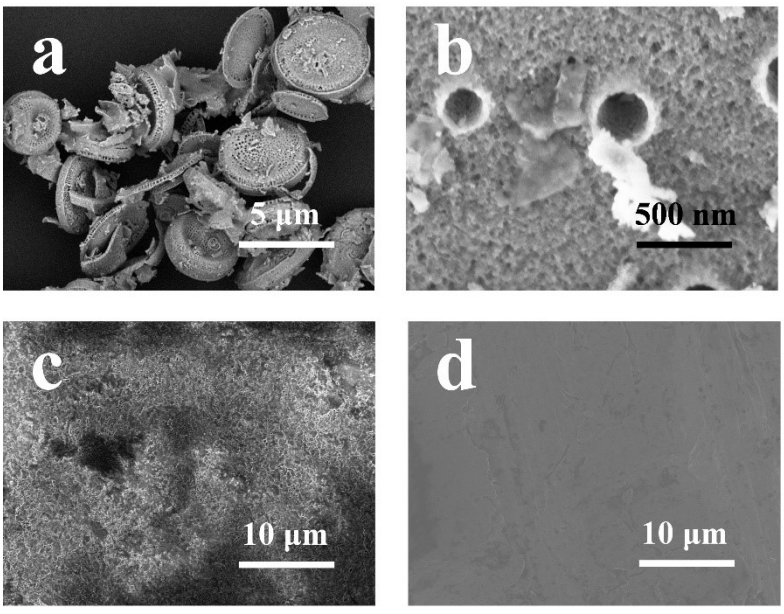

Fig. S5 SEM images of (a, b) DTM/A, (c) DTM/A-Zn, and (d) bare Zn.

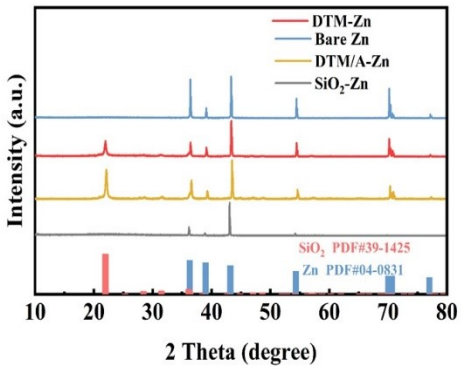

Fig. S6 XRD patterns of bare Zn, DTM-Zn, DTM/A-Zn, and SiO_2-Zn.

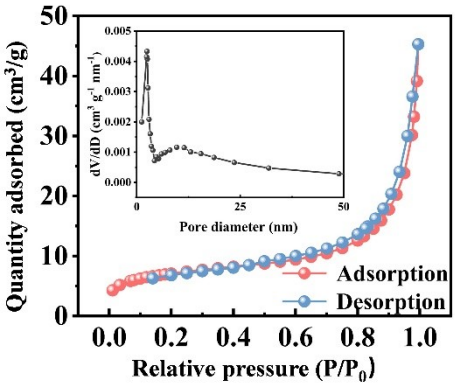

Fig. S7 N_2 adsorption-desorption isotherm and pore size distribution of the DTM/A.

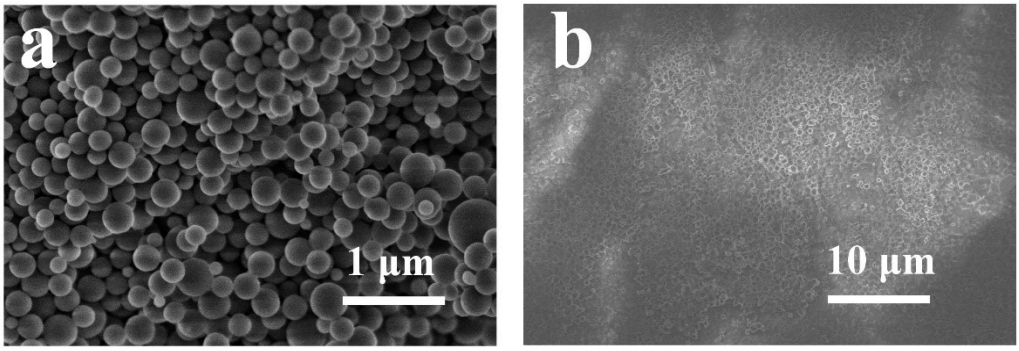

Fig. S8 SEM images of (a) SiO_2 nanoparticles and (b) SiO_2-Zn.

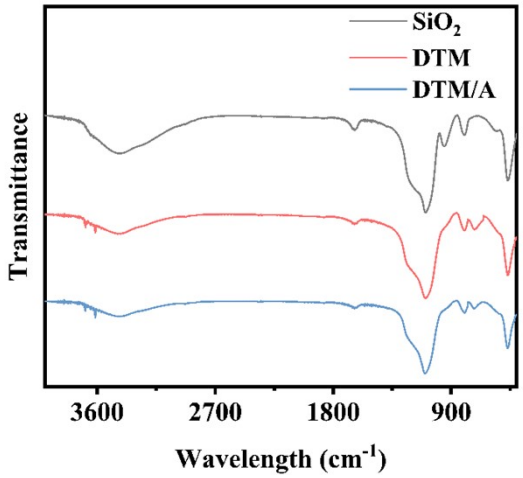

Fig. S9 FTIR spectra of DTM, DTM/A, and SiO_2.

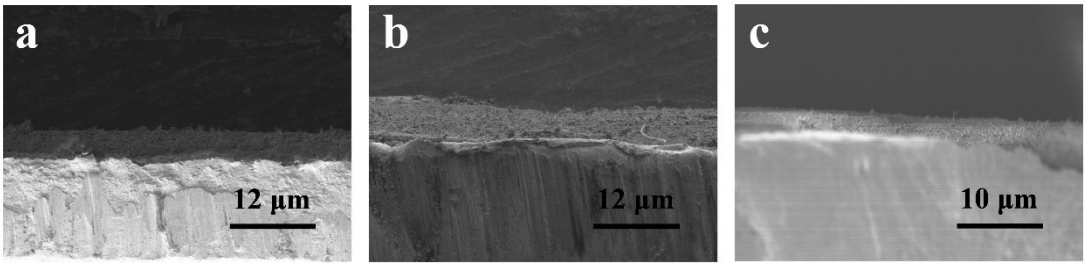

Fig. S10 Cross-section SEM images of (a) DTM-Zn, (b) DTM/A-Zn, and (c) SiO_2-Zn.

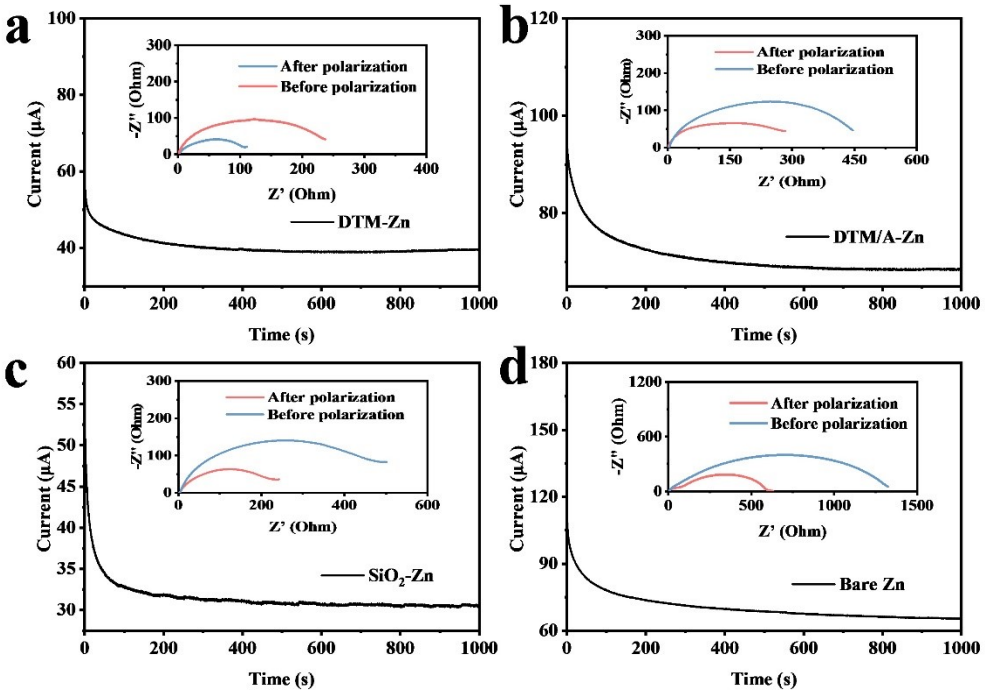

Figure S11 Current-time plots of (a) DTM-Zn, (b) DTM/A-Zn, (c) SiO_2-Zn, and (d) bare Zn symmetric cells. The insets show the impedance spectra before and after polarization. The transference number of Zn^{2+} can be calculated by the following formula:

$$T_{Zn^{2+}} = \frac{I_S(\Delta V - I_0 R_0)}{I_0(\Delta V - I_S R_S)}$$

where ΔV is the applied voltage; I_0 and R_0 are the initial current and resistance, respectively; I_S and R_S are the steady-state current and resistance, respectively.

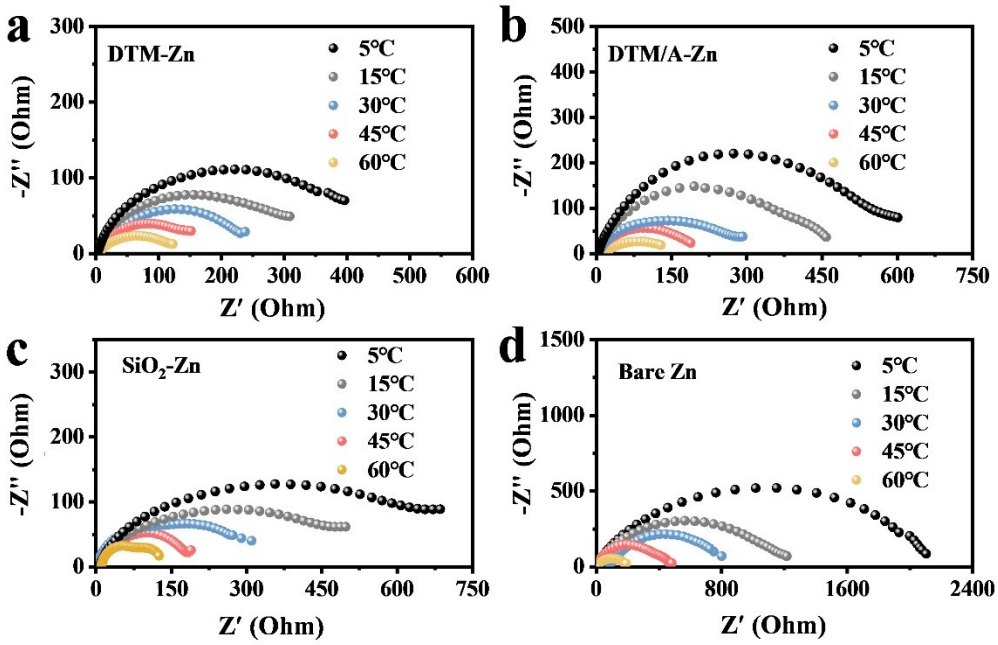

Figure S12 Arrhenius activation energy (Ea) of the desolventizing steps of (a) DTM-Zn, (b) DTM/A-Zn, (c) SiO_2-Zn, and (d) bare Zn symmetric cells.

Ea can be approximated as the desolvating energy barrier for hydrated Zn^{2+}, which can be calculated according to the following Arrhenius equation:

$1/Rct = Aexp(-Ea /RT)$

Where Rct, A, R, and T represent the charge-transfer resistance, frequency factor, gas constant, and absolute temperature, respectively. EIS profiles of the four electrodes at different temperatures from 5 to 60 ºC were tested.

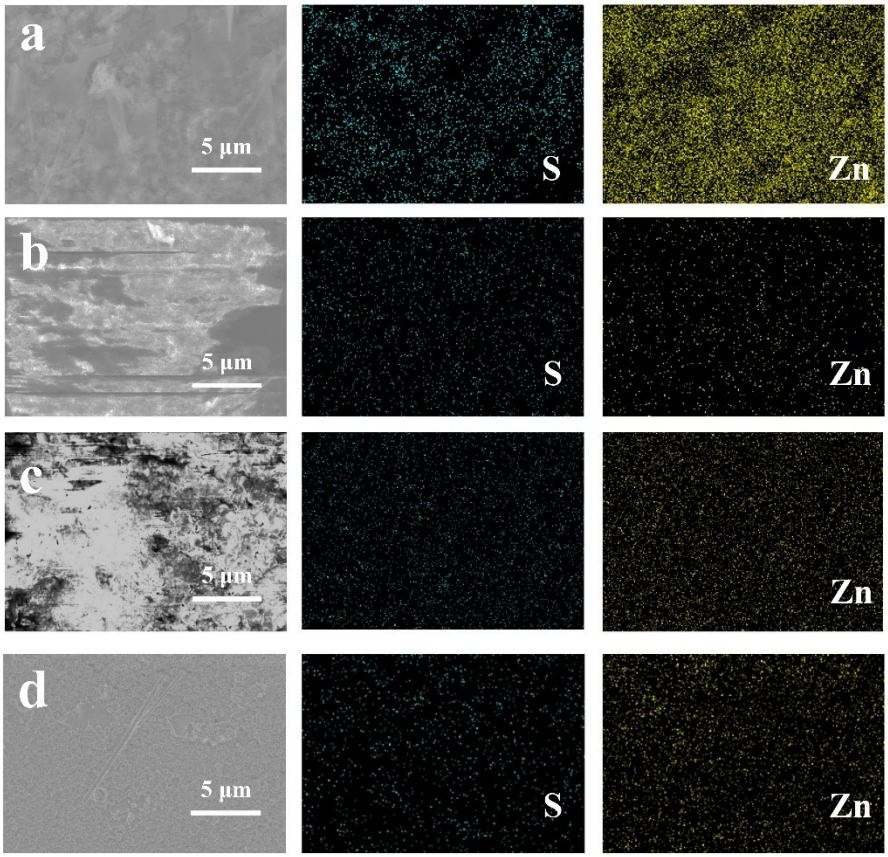

Fig. S13 SEM and mapping results of (a) bare Zn, (b) DTM-Zn, (c) DTM/A-Zn, and (d) SiO_2-Zn after immersion in the electrolyte for 7 days.

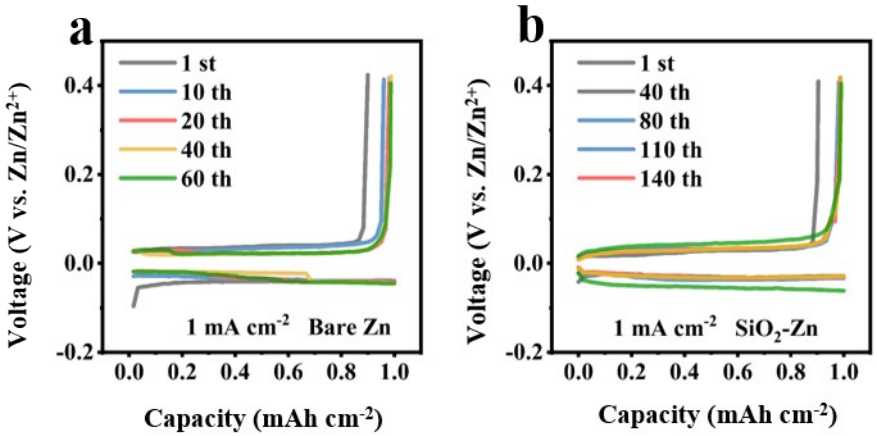

Fig. S14 Voltage profiles at selected cycles of (a) bare Zn and (b) SiO_2-Zn cells.

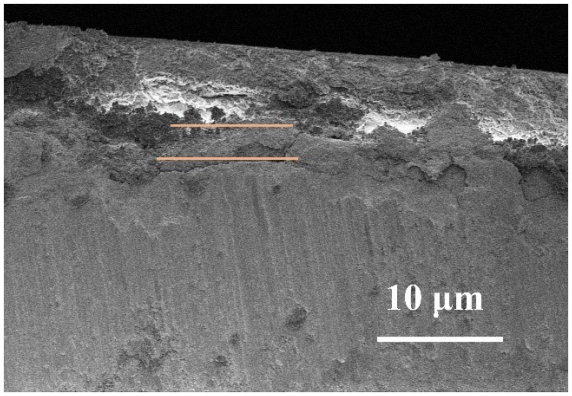

Fig. S15 The cross-section SEM image of DTM-Zn after depositing zinc.

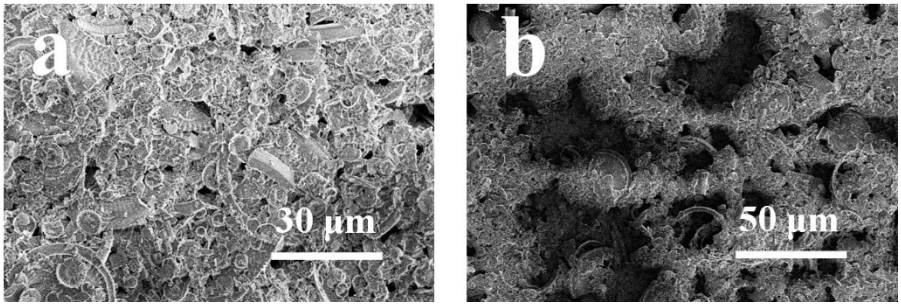

Fig. S16 SEM images of DTM-Zn without pressure treatment (a) before and (b) after depositing zinc.

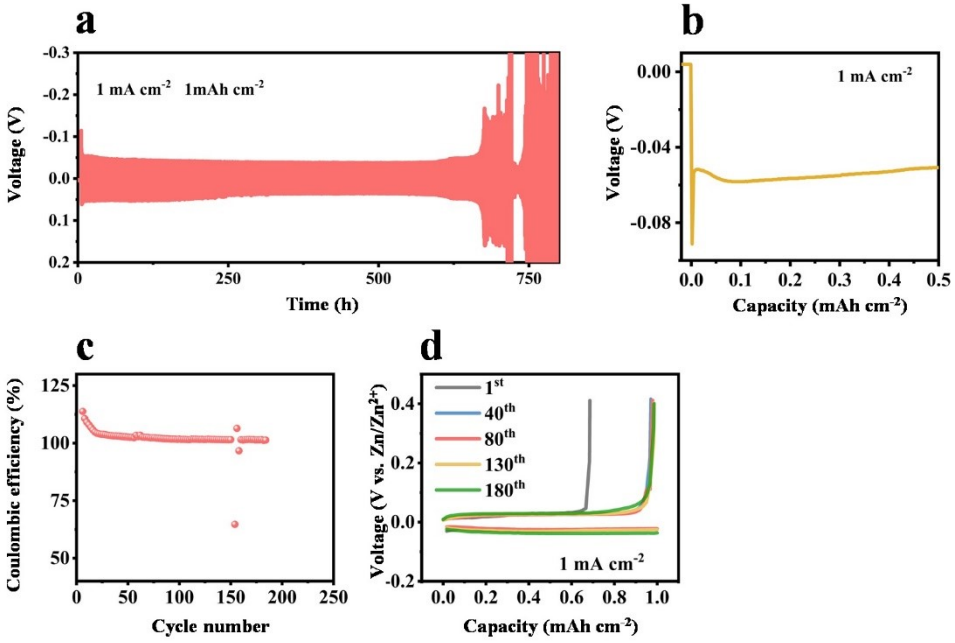

Fig. S17 (a) Long-term cycling at 1 mA cm^{-2}, (b) Nucleation overpotential at 1 mA

cm^{-2}, (c) Coulombic efficiency, and (d) Voltage profiles at selected cycles of DTM-Zn (without pressure treatment).

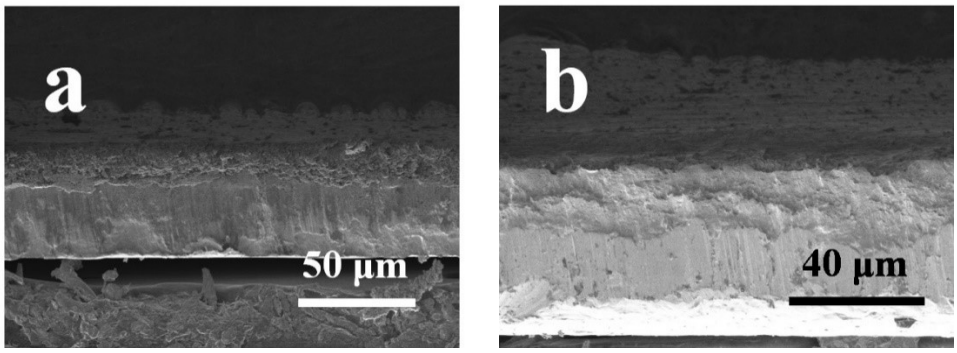

Fig. S18 SEM images of (a) DTM-Zn (10 μm) and (b) DTM-Zn (2 μm).

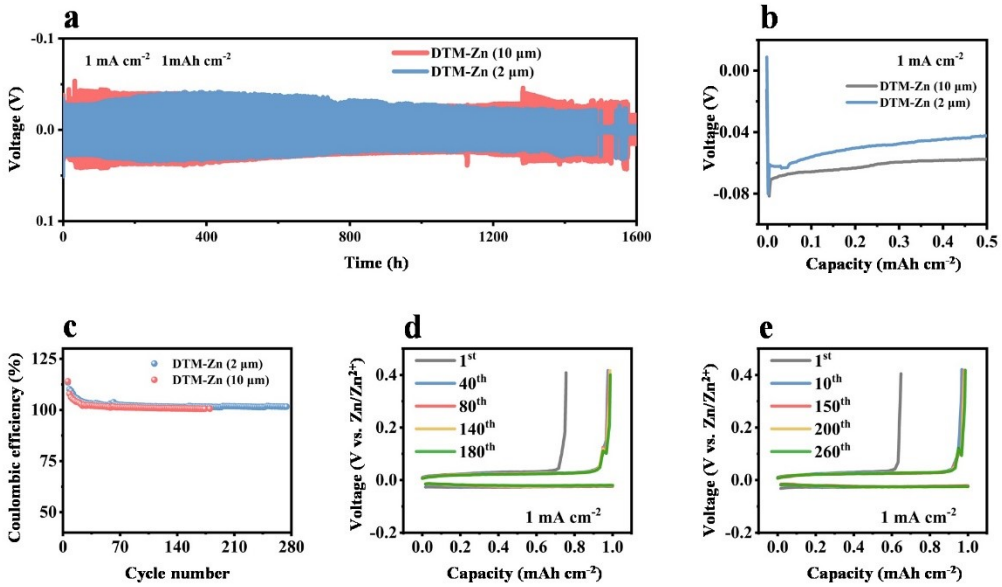

Fig. S19 (a) Long-term cycling at 1 mA cm^{-2}, (b) Nucleation overpotential at 1 mA cm^{-2}, and (c) Coulombic efficiency of DTM-Zn (2 μm and 10 μm). Voltage profiles at selected cycles of (d) DTM-Zn (10 μm) and (e) DTM-Zn (2 μm).

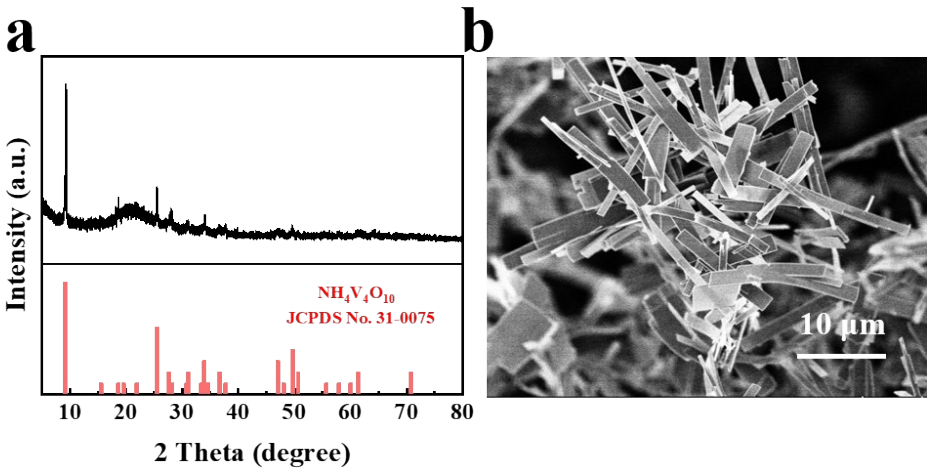

Fig. S20 (a) XRD pattern and (b) SEM image of $NH_4V_4O_{10}$.

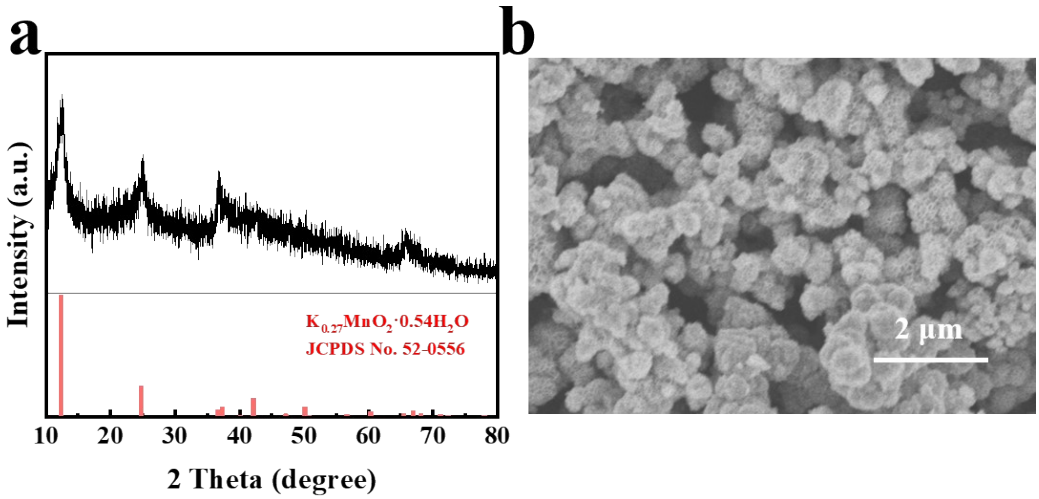

Fig. S21 (a) XRD pattern and (b) SEM image of KMO.

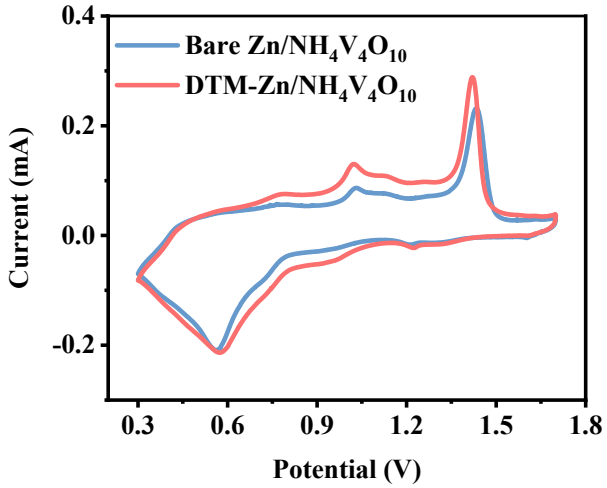

Fig. S22 CV curves of Bare $Zn/NH_4V_4O_{10}$ and DTM-$Zn/NH_4V_4O_{10}$.

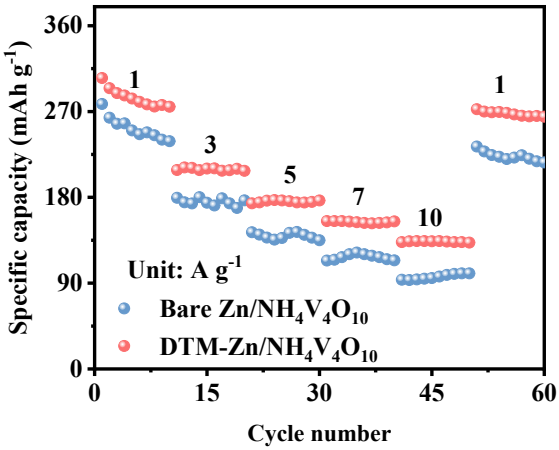

Fig. S23 Rate performance of Bare $Zn/NH_4V_4O_{10}$ and DTM-$Zn/NH_4V_4O_{10}$.

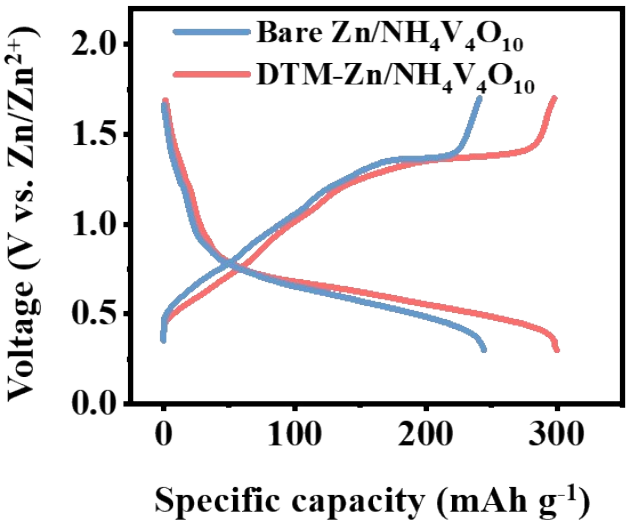

Fig. S24 Charge and discharge curves of Bare $Zn/NH_4V_4O_{10}$ and DTM-$Zn/NH_4V_4O_{10}$.

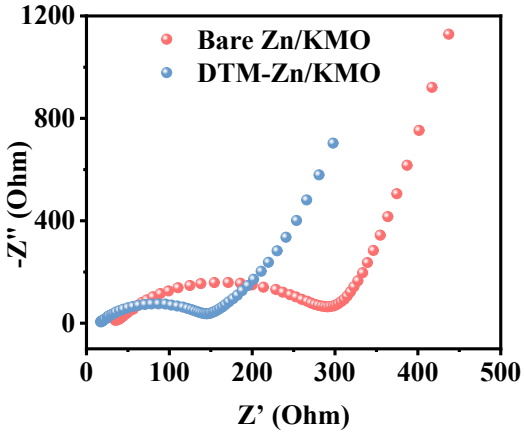

Fig. S25 EIS plots of DTM-Zn/KMO and Bare Zn/KMO cells.

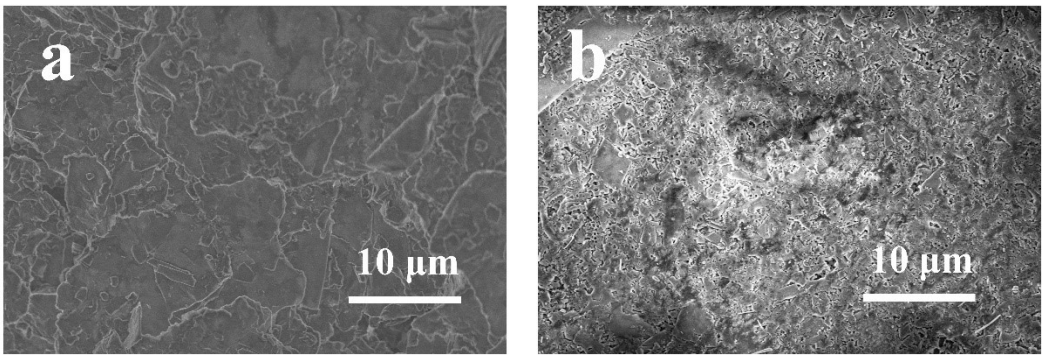

Figure S26 SEM images of (a) bare Zn and (b) DTM-Zn in Zn/KMO cells after 500 cycles.

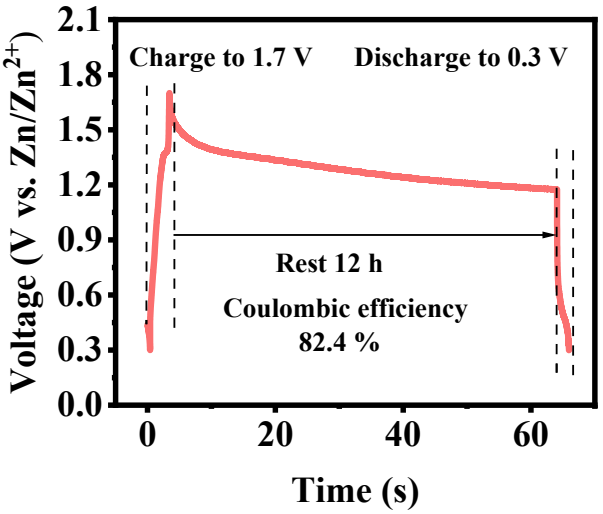

Fig. S27 Self-discharge curve of Bare Zn/$NH_4V_4O_{10}$ cells.

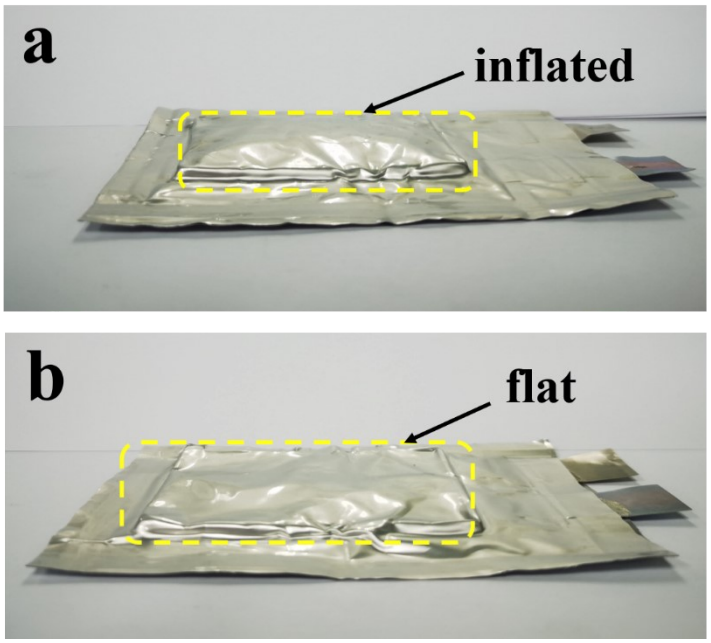

Fig. S28 Pouch cells with (a) bare Zn and (b) DTM-Zn after cycling.

Table S1. Comparison of main parameters and cycling property for this work with other previous works.

Electrode	**Current density (mA cm^{-2})**	**Areal capacity (mAh cm^{-2})**	**Cycling life (h)**	**Ref**
PASM-Zn	1	1	900	[1]
Zn@PCFs	1	5	1500	[2]
NGO@Zn	0.5	0.25	2200	[3]
DES-Zn	3	2	800	[4]
$ZnSO_4$+Arg	1	10	300	[5]
ADC-gel	5	5	650	[6]

E-nHAP@Zn	10	5	400	[7]
MTSi-Hedp-Zn	1	1	1250	[8]
DTM-Zn	**1**	**0.5**	**3200**	**This work**
	10	**10**	**650**	**This work**

References

[1] N. Wang, Z. Wu, Y. Long, D. Chen, C. Geng, X. Liu, D. Han, J. Zhang, Y. Tao, Q.-H. Yang, MXene-assisted polymer coating from aqueous monomer solution towards dendrite-free zinc anodes, J. Energy Chem. 73 (2022) 277-284, https://doi.org/10.1016/j.jechem.2022.06.009.

[2] H. Ying, P. Huang, Z. Zhang, S. Zhang, Q. Han, Z. Zhang, J. Wang, W.-Q. Han, Freestanding and flexible interfacial layer enables bottom-up Zn deposition toward dendrite-free aqueous Zn-ion batteries, Nano-Micro Lett. 14 (2022) 180, https://doi.org/10.1007/s40820-022-00921-6.

[3] Y. Li, D. Zhao, J. Cheng, Y. Lei, Z. Zhang, W. Zhang, Q. Zhu, A bifunctional nitrogen doped carbon network as the interlayer for dendrite-free Zn anode, Chem. Eng. J. 452 (2023) 139264, https://doi.org/10.1016/j.cej.2022.139264.

[4] M. Kwon, J. Lee, S. Ko, G. Lim, S.-H. Yu, J. Hong, M. Lee, Stimulating Cu–Zn alloying for compact Zn metal growth towards high energy aqueous batteries and hybrid supercapacitors, Energy Environ. Sci. 15 (2022) 2889-2899, https://doi.org/10.1039/D2EE00617K.

[5] H. Lu, X. Zhang, M. Luo, K. Cao, Y. Lu, B.B. Xu, H. Pan, K. Tao, Y. Jiang, Amino

acid-induced interface charge engineering enables highly reversible Zn anode, Adv. Funct. Mater. 31 (2021) 2103514,https://doi.org/10.1002/adfm.202103514.

[6] Q. He, G. Fang, Z. Chang, Y. Zhang, S. Zhou, M. Zhou, S. Chai, Y. Zhong, G. Cao, S. Liang, A. Pan, Building ultra-stable and low-polarization composite Zn anode interface via hydrated polyzwitterionic electrolyte construction, Nano-Micro Lett. 14 (2022) 93, https://doi.org/10.1007/s40820-022-00835-3.

[7] K. Qi, W. Zhu, X. Zhang, M. Liu, H. Ao, X. Wu, Y. Zhu, Enamel-like layer of nanohydroxyapatite stabilizes Zn metal anodes by ion exchange adsorption and electrolyte pH regulation, ACS Nano 16 (2022) 9461-9471, https://doi.org/10.1021/acsnano.2c02448.

[8] H. Yu, Y. Chen, H. Wang, X. Ni, W. Wei, X. Ji, L. Chen, Engineering multi-functionalized molecular skeleton layer for dendrite-free and durable zinc batteries, Nano Energy 99 (2022) 107426, https://doi.org/10.1016/j.nanoen.2022.107426.